Supplementary material

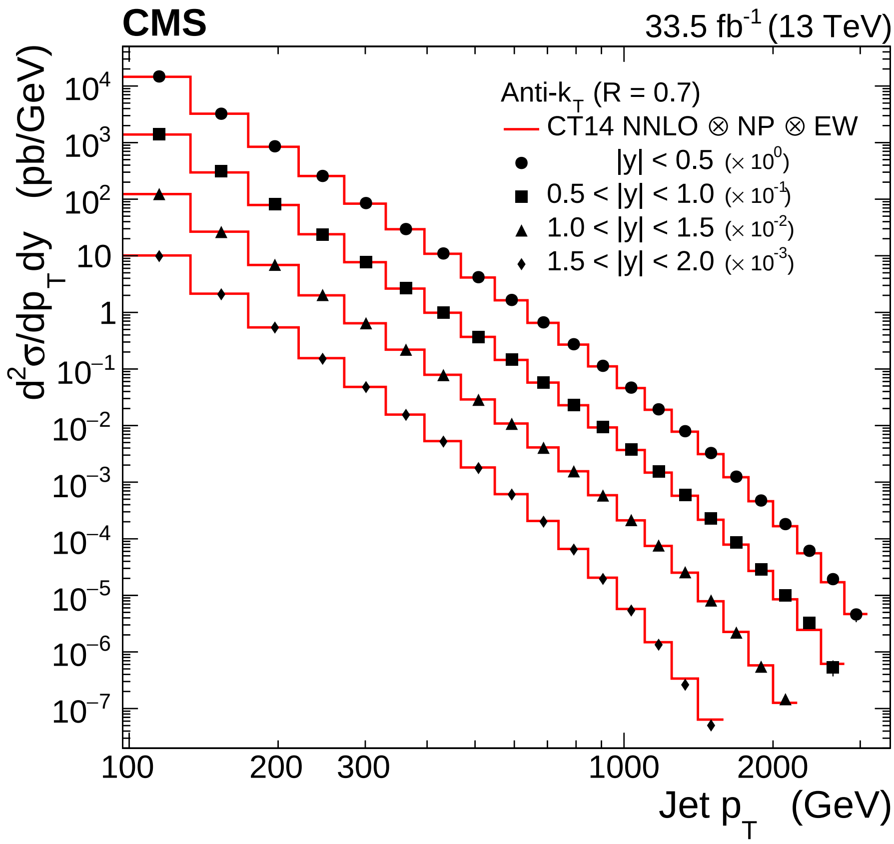

From Fig. 6 in Ref. [2]: Double-differential inclusive jet cross sections measured for jets with $R = 0.7$.

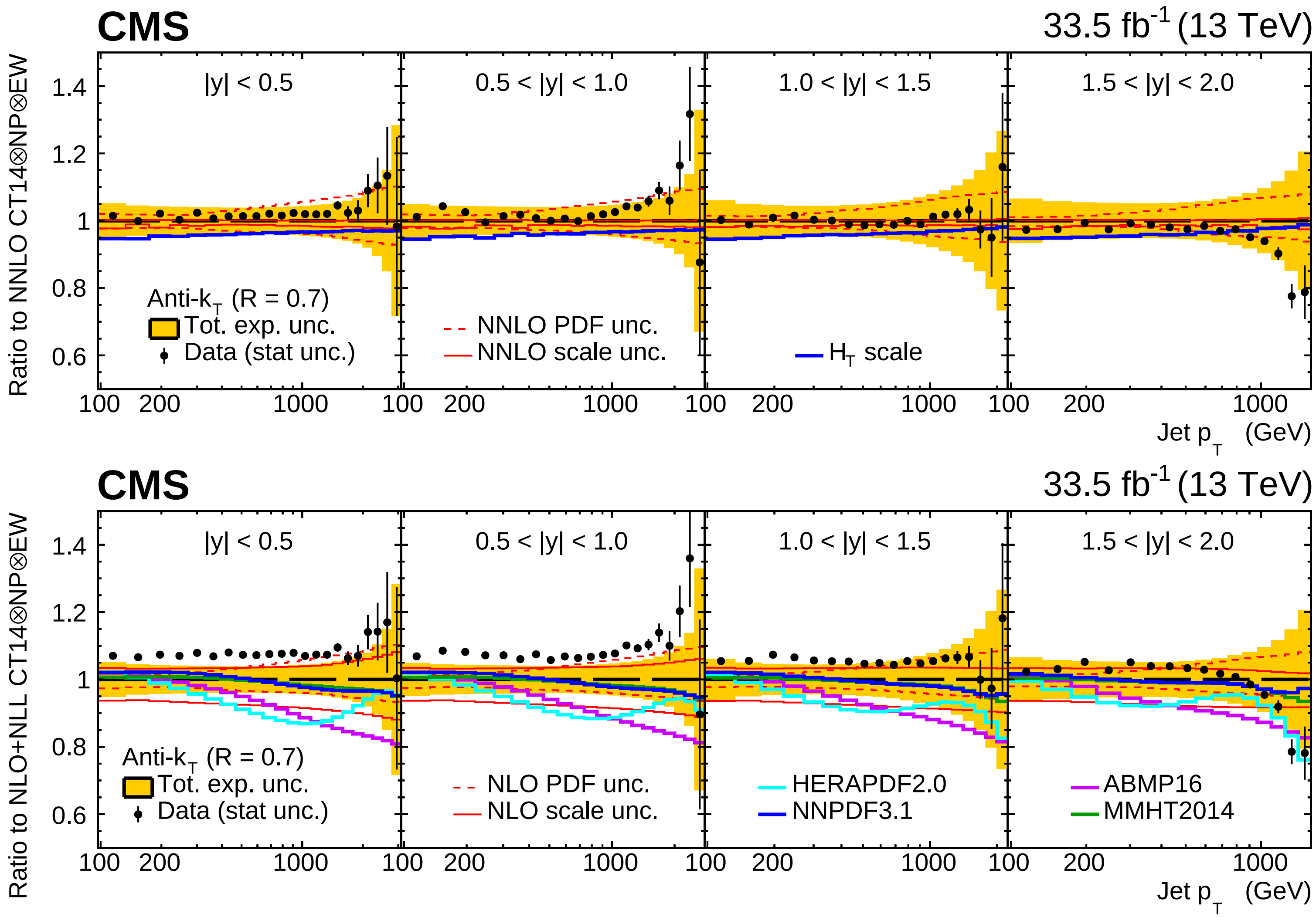

From Fig. 8 in Ref. [2]: Ratio of measured cross sections to fixed-order theoretical predictions at NNLO (upper) and NLO+NLL (lower), corrected for NP and EW effects.

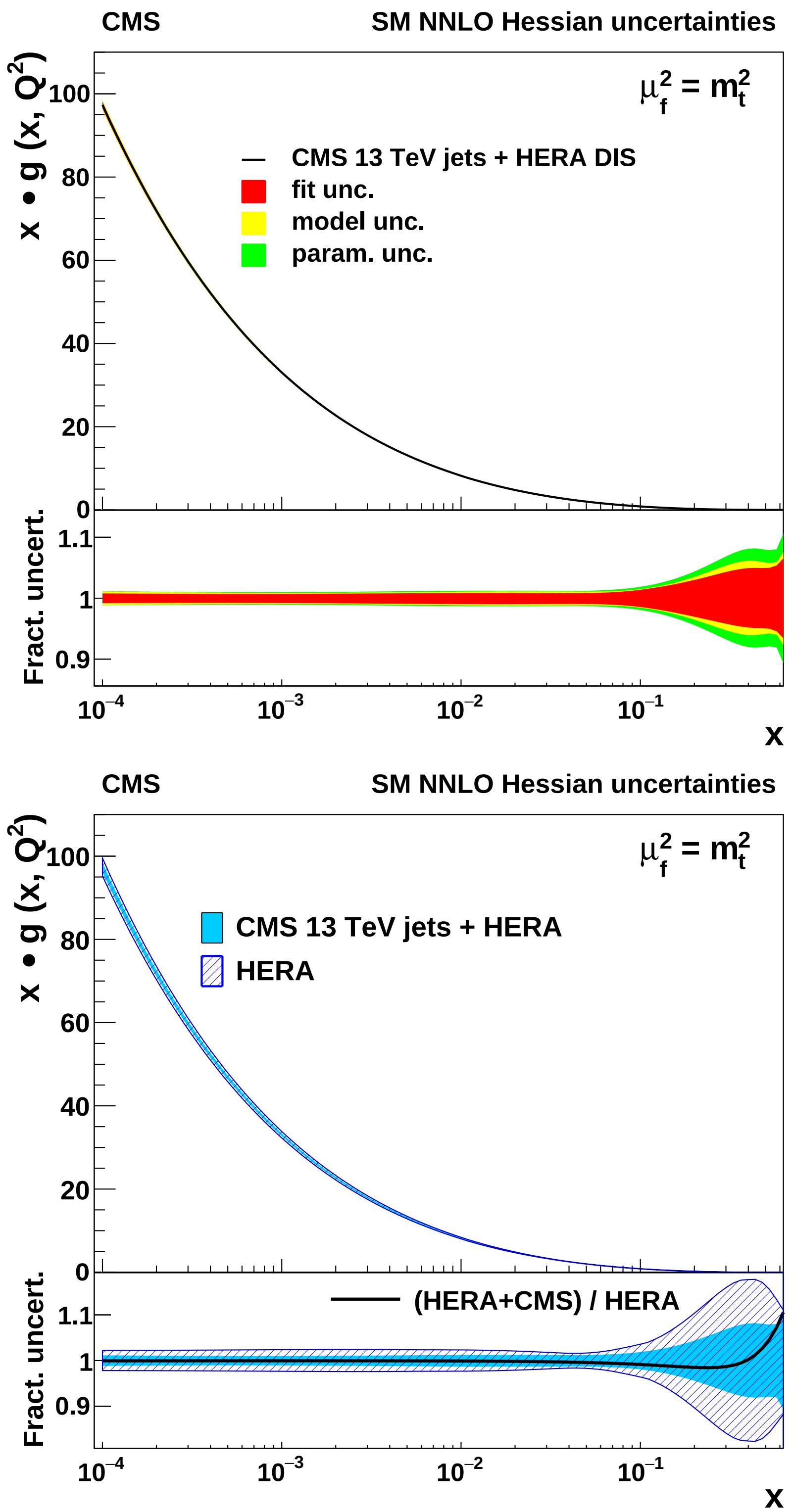

From Figs. 14 and 15 in Ref. [2]: Gluon PDF and uncertainties obtained in the fit to the HERA and CMS inclusive jet data (upper), and compared to the fit using only HERA data (lower).

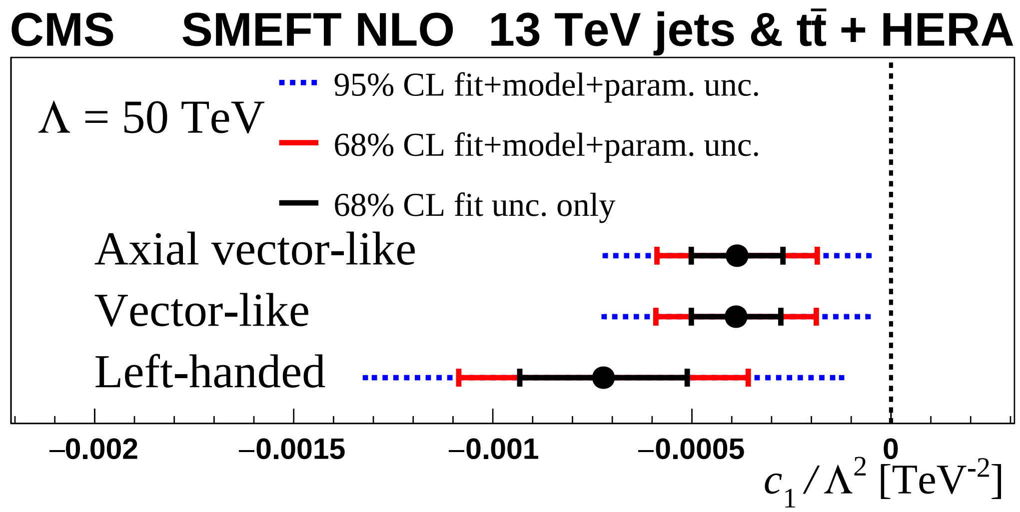

From Fig. 19 in Ref. [2]: Limits on Wilson coefficients for four-quark contact interactions in Standard Model effective field theory.

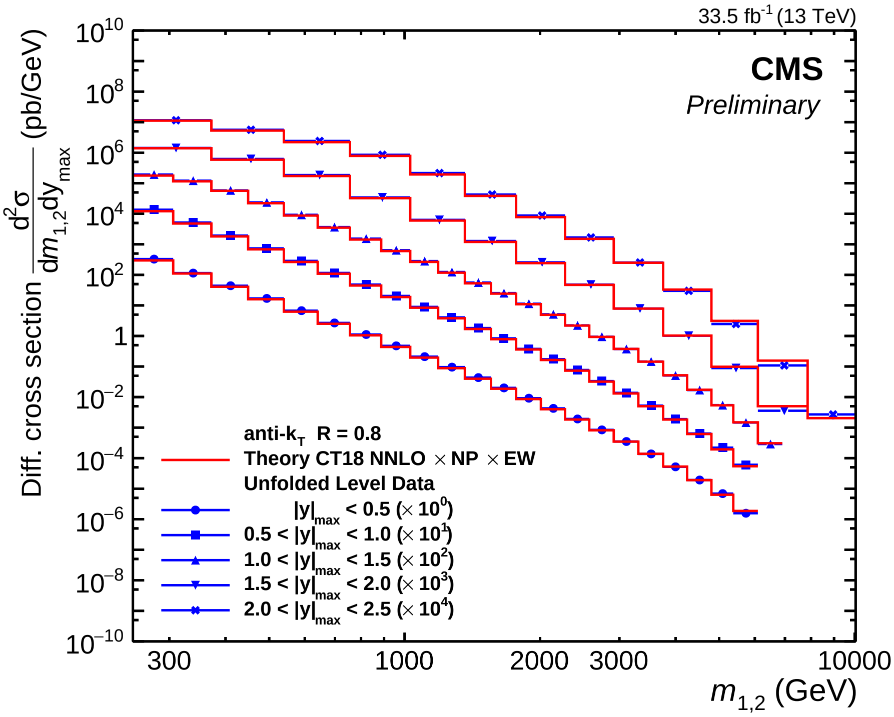

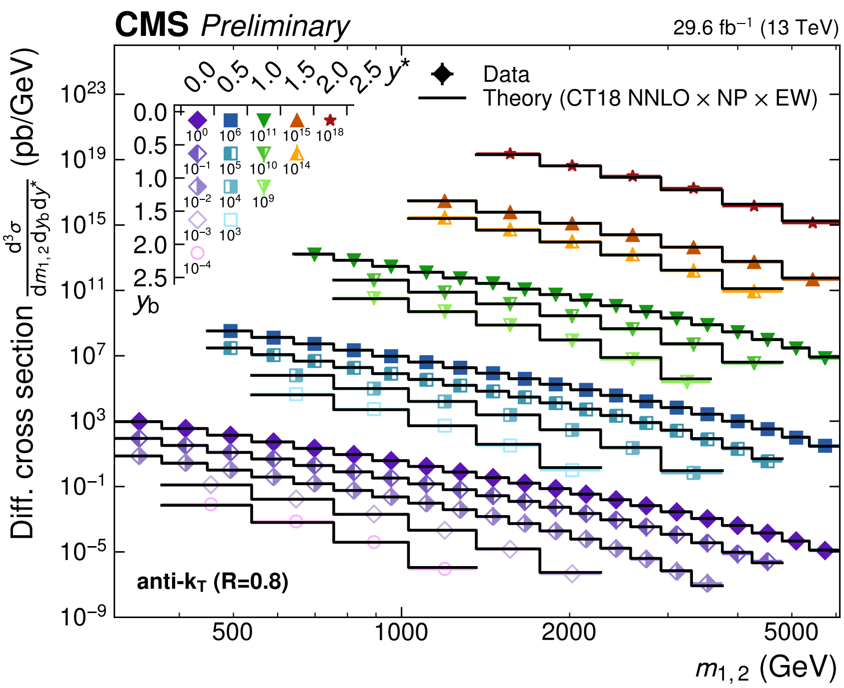

From Figs. 8 and 19 in Ref. [3]: Double- (upper) and triple-differential (lower) dijet cross sections measured for jets with $R = 0.8$.

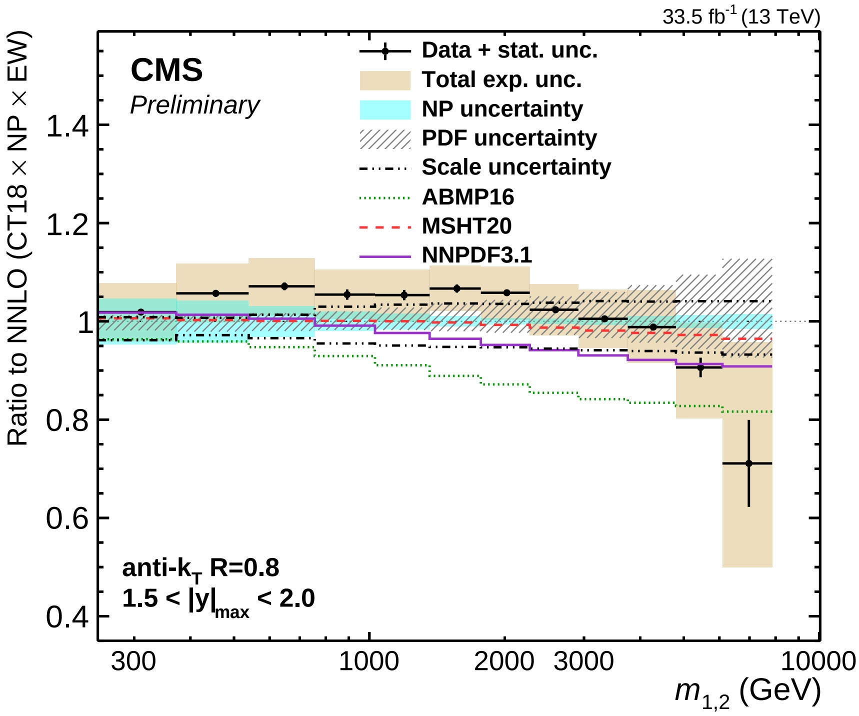

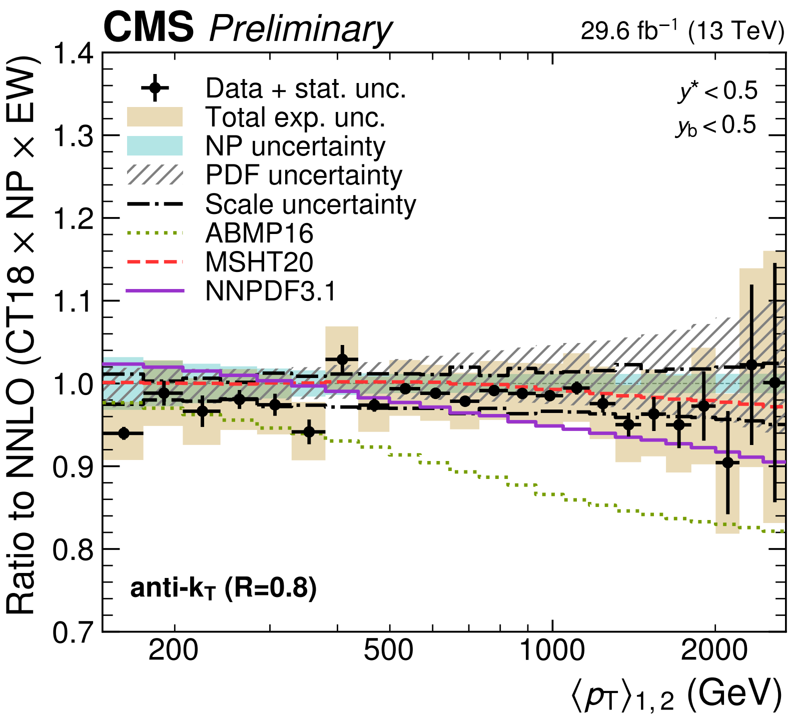

From Figs. 26 and 10 in Ref. [3]: Ratio of measured double- (upper) and triple-differential (lower) cross sections to fixed-order theoretical predictions at NNLO for jets with $R = 0.8$.

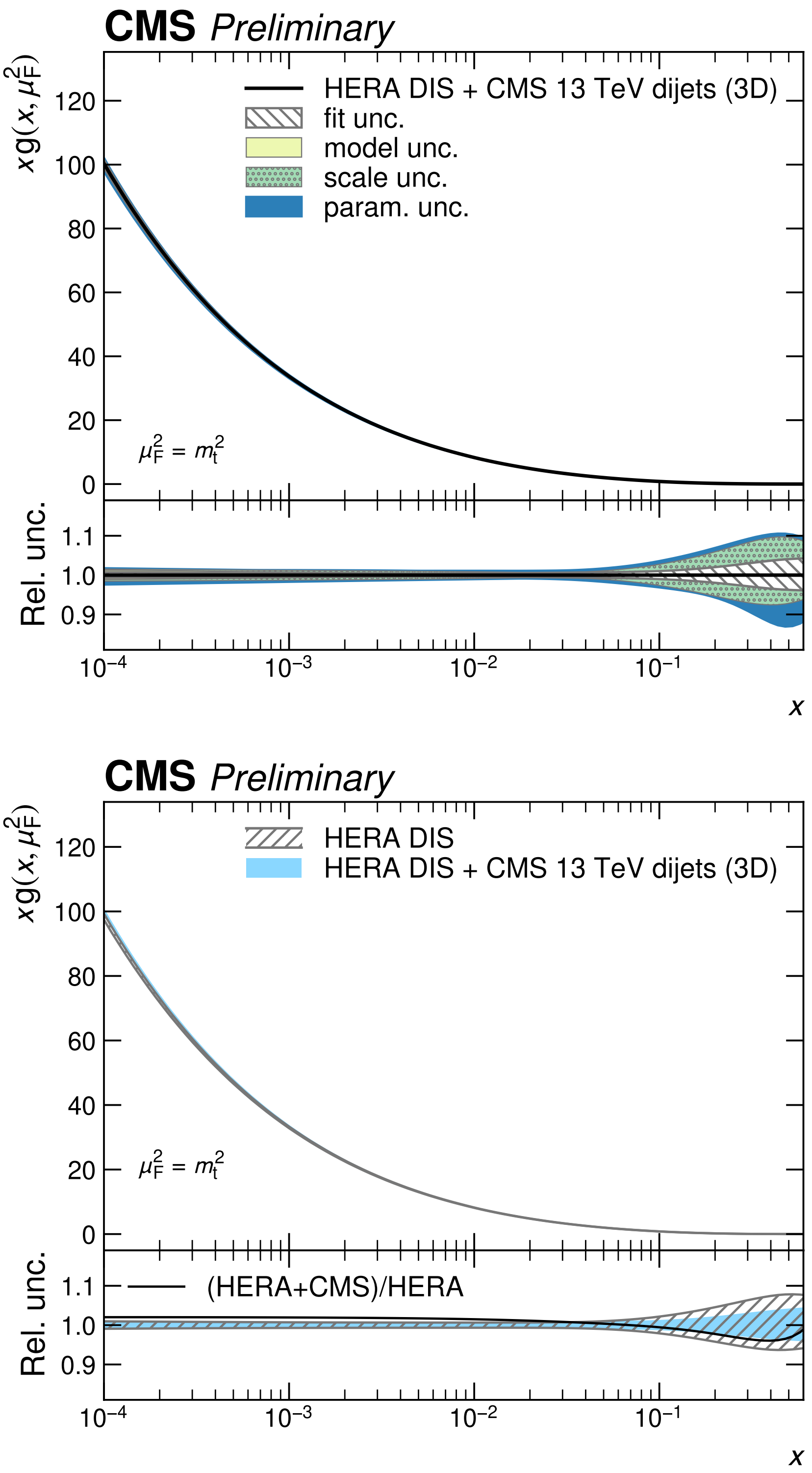

From Figs. 12 and 14 in Ref. [3]: Gluon PDF and uncertainties obtained in the fit to the HERA and CMS 3D dijet data (upper), and compared to the fit using only HERA data (lower).

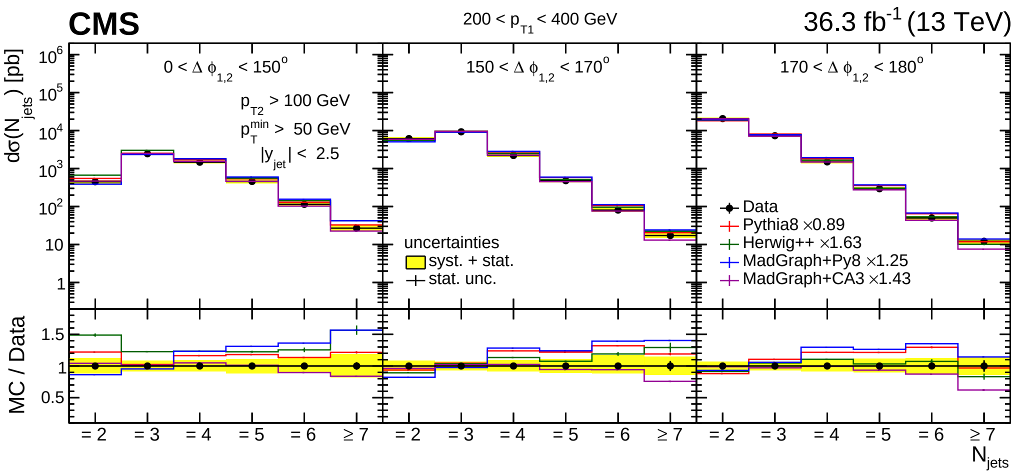

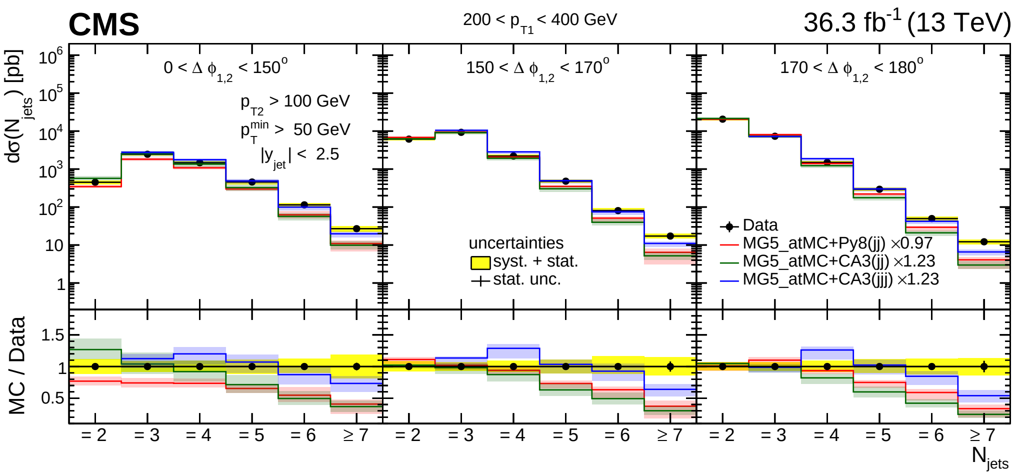

From Figs. 8 and 9 in Ref. [4]: Comparison of measured jet multiplicity distributions to predictions from MC event generators at LO (upper) and NLO (lower). The distributions illustrated here include events with a leading jet transverse momentum satisfying $200 < p_{\mathrm{T}} < 400\,\mathrm{GeV}$ and are shown for three regions of the azimuthal angle separation $\Delta\phi$.

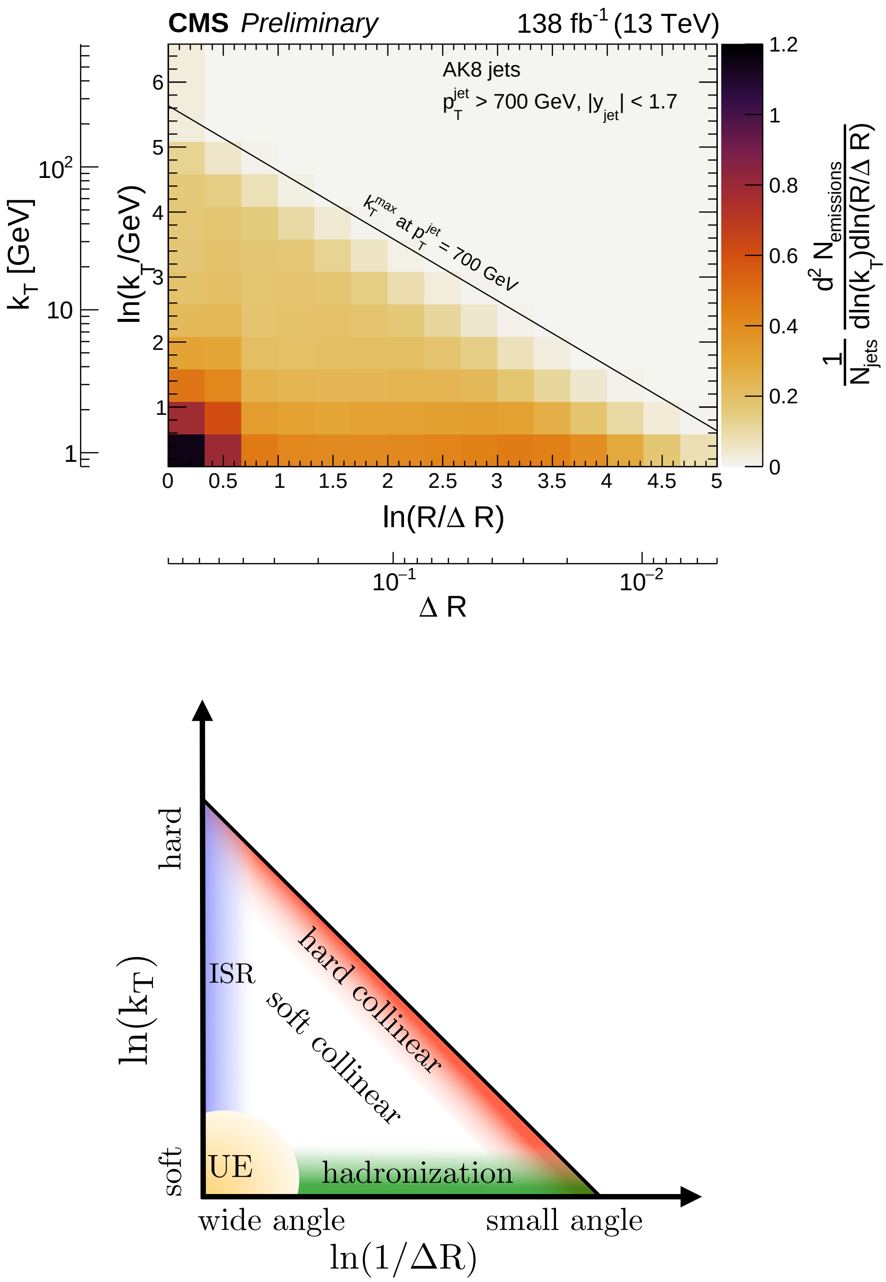

From Figs. 7 and 2 in Ref. [13]: Two-dimensional primary Lund jet plane density (upper) and a schematic representation of the regions affected by different physical effects (lower).

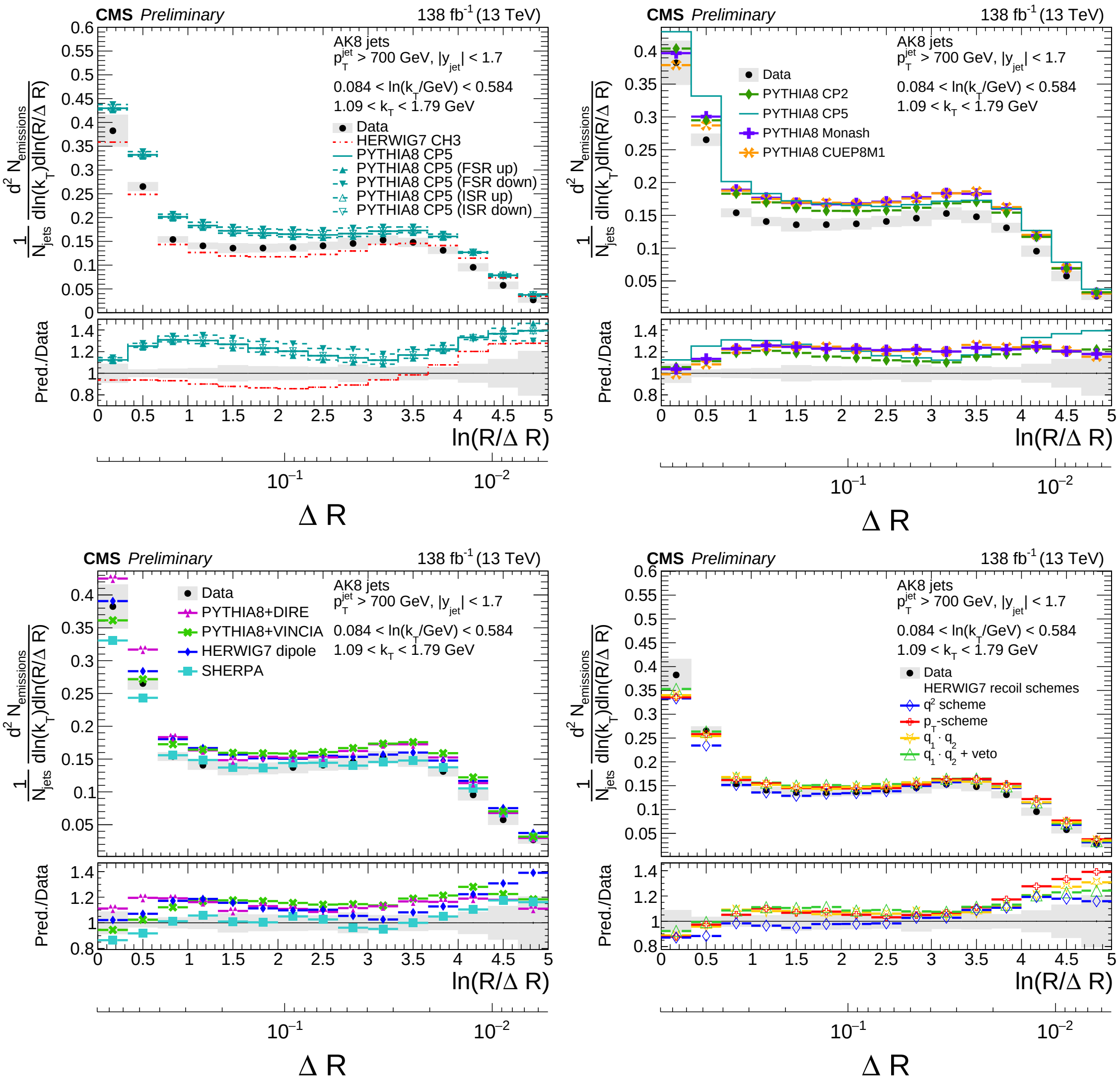

From Figs. 9–12 in Ref. [13]: Comparison of data to predictions obtained with different MC generators (upper left), tunes (upper right), parton shower models (lower left), and HERWIG 7 recoil schemes (lower right), illustrated here as a function of the emission angle in the low-k_T region of the primary Lund jet plane.